Milligram-Scale High-Voltage Power Electronics for Piezoelectric Microrobots

Michael Karpelson, *Student Member, IEEE,* Gu-Yeon Wei, *Member, IEEE,* Robert J. Wood, *Member, IEEE*

***Abstract*— Piezoelectric actuators can achieve high efficiency and power density in very small geometries, which shows promise for microrobotic applications, such as flapping-wing robotic insects. From the perspective of power electronics, these actuators present two challenges: high operating voltages, ranging from tens to thousands of volts; and a low electromechanical coupling factor, which necessitates the recovery of unused electrical energy. This paper explores the power electronics design problem by establishing the drive requirements of piezoelectric actuators, presenting circuit topologies and control methods suitable for driving different types of piezoelectric actuators in microrobotic applications, and demonstrating experimental realizations of sub-100mg power electronics circuits.**

***Index Terms*— microrobots, piezoelectric actuator, power electronics**

I. Introduction

Highly compact yet powerful actuators are crucial in many robotics applications, particularly small-scale autonomous systems such as bio-inspired microrobots. In recent years, a number of actuation methods have been proposed or applied in a microrobotic context, including piezoelectric [1], electrostatic [2], and dielectric elastomer actuators [3]. These actuation methods have the potential to achieve high efficiencies and high power densities in very small geometries. Piezoelectric actuators in particular have shown promise in applications with very stringent weight and power density requirements, such as the Harvard Microrobotic Fly (HMF) – a flapping-wing robotic insect capable of liftoff with external power [4].

In order to produce mechanical output, the actuation methods mentioned above rely on the presence of electric charge on various conductive surfaces in order to either generate high electric fields, as in the case of piezoelectric actuators, or high electrostatic forces, as in the case of electrostatic and dielectric elastomer actuators. Moreover, the geometries of such actuators inherently produce significant electrical capacitance, and therefore high operating voltages are usually necessary to accumulate a sufficient amount of electric charge on the actuator electrodes, ranging from tens to thousands of volts. For example, the piezoelectric actuators used in the HMF require drive voltages in the range of 200-300V. There are two major challenges in the design of power electronics capable of driving capacitive actuators: generating high voltages from low-voltage sources, and recovering unused energy from the actuator.

The authors are with the School of Engineering and Applied Sciences, Harvard University, Cambridge, MA 02138, USA (contact e-mail: michaelk@seas.harvard.edu)

Most compact energy sources suitable for microrobotic applications, such as lithium batteries, supercapacitors [5], solar cells [6], or fuel cells [7], generate output voltages below 5V. Connecting many such cells in series to obtain high voltage is generally not practical because the packaging overhead causes a significant reduction in energy density. Consequently, the generation of high voltages for HMF actuators requires voltage conversion circuits with step-up ratios ranging from 50 to 100. While there are a number of circuit topologies with high step-up ratios, many of them cannot be easily miniaturized and/or suffer from poor efficiency at the low output power levels common in microrobotic applications. Careful selection and optimization of the conversion circuit is necessary to ensure that heavy, inefficient electronics do not compromise system performance.

In addition to the voltage step-up functionality, the power electronics circuitry must generate a time-varying signal on the input electrodes of the actuator. The second challenge stems from the fact that, depending on the properties of the actuator, the nature of the mechanical load, and the characteristics of the drive signal, only a small fraction of the electrical energy stored in the actuator is converted into useful mechanical output [8]. In order to maximize overall system efficiency, it is highly desirable to both generate an appropriate drive signal and recover as much of the unused energy as possible, which imposes additional requirements on the drive circuitry.

This paper describes promising power electronics circuits that can generate the high, time-varying voltages necessary for the operation of piezoelectric actuators, while meeting the stringent weight requirements of microrobotic systems and maximizing system efficiency. Although the analysis focuses on piezoelectric actuators, many of the concepts described here can easily be adapted to other high-voltage capacitive actuators, such as electrostatic comb drives or dielectric elastomer actuators. This work reviews the electrical properties and drive requirements of piezoelectric actuators (Section II), and presents power electronics circuits applicable to various types and configurations of piezoelectric actuators (Sections III and IV). Experimental realizations of the drive circuits are described (Section V), including applications to milligram-scale microrobots, such as flapping-wing robotic insects.

II. Piezoelectric Actuator Drive Requirements and Methods

Piezoelectric actuators are available in many configurations, including linear devices such as stack actuators

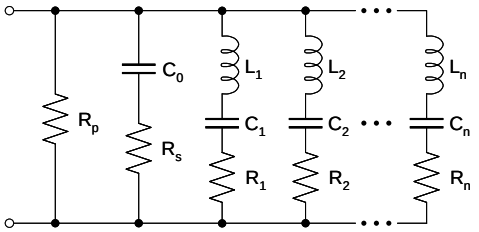

Fig. 1. Piezoelectric element equivalent circuit.

TABLE I
EQUIVALENT CIRCUIT PARAMETERS OF BIMORPH ACTUATOR

Static parameters	Value	Dynamic parameters	Mode 1	Mode 2
C_0	14.5nF	L_i	3.52kH	1.03kH
R_s	100Ω	C_i	2nF	0.8nF
R_p	10MΩ	R_i	130kΩ	38kΩ

and bending devices such as unimorph and bimorph cantilevers [9]. In order to establish the requirements for the power electronics circuits, it is important to understand the electrical response of the actuator and the nature of the drive signal. This section describes the equivalent circuit representation of piezoelectric actuators and driving methods that can maximize system efficiency.

A. Piezoelectric Actuator Equivalent Circuit

In the electrical domain, a piezoelectric element can be represented with an equivalent circuit where impedance is linked to the mechanical properties of the actuator and its load. The Van Dyke circuit model, adopted by the IEEE Standard on Piezoelectricity, is the best known circuit, although various enhancements to this circuit have been proposed to better represent the nonlinear effects of piezoelectric actuators [10], [11].

This paper adopts the equivalent circuit of [10], shown in Fig. 1. The circuit can be divided into a static part, which represents the primary capacitance by C_0, dielectric losses by R_p, and hysteresis losses by R_s, and a number of resonant branches, each corresponding to a mechanical vibration mode. In each branch, L_i, R_i, and C_i represent the equivalent mass, damping coefficient, and spring constant, respectively, of the vibration mode. Although hysteresis, as a nonlinear loss mechanism, cannot be fully represented by linear circuit components, the equivalent circuit parameters can be chosen to provide a good approximation of the hysteresis losses for a given drive voltage and operating frequency [8].

The equivalent circuit can adequately represent a dual-electrode piezoelectric actuator, such as a stack or unimorph bending actuator, or a single piezoelectric element in a multi-electrode actuator such as a bimorph. Table I shows some of the parameters for a typical bimorph bending actuator connected to the wings of the HMF, including the first two resonant modes.

B. Drive Circuit Requirements

In order to ensure adequate actuator performance and maximize efficiency, the high-voltage drive circuit must produce an output signal that is unipolar and sinusoidal. In addition, it must be capable of recovering unused energy from the actuator.

Piezoelectric actuators may be driven with either a bipolar or unipolar signal. In bipolar driving, the drive voltage varies between a positive or negative voltage, which can result in either expansion or contraction of the driven piezoelectric element. In unipolar driving, the voltage is only positive, resulting in contraction only. In microrobotic applications such as [4] or [12], piezoelectric actuators provide power for locomotion, which requires large strains and therefore high actuation voltages to enable large wing or leg strokes. Since high-amplitude bipolar drive signals can result in the depolarization of the piezoelectric element, the drive signal must be unipolar.

In the HMF, piezoelectric actuators are driven at a frequency close to the lowest mechanical vibration mode, corresponding to the flapping motion of the wings [4], in order to amplify the wing stroke. However, as evident from Table I, there is more than one mechanical vibration mode present in the system. These modes do not contribute to wing motion but are nevertheless capable of storing and dissipating energy. As a result, it is desirable to minimize the amount of energy that couples into these modes or, equivalently, the amount of energy coupled into the corresponding LCR branches of the circuit model. A sinusoidal drive signal, which concentrates all energy at a single frequency, can fulfill this requirement.

The equivalent circuit also shows that the majority of the energy stored in the actuator remains in the primary capacitance C_0 (in fact, the values of the capacitors C_0 and C_1 through C_n are proportional to the amount of energy that, for a given operating voltage, can be stored in the primary capacitance and the vibration modes). As noted in [8], this energy is recoverable, and therefore the drive circuit should be capable of returning this energy to the supply or to a second piezoelectric layer that is activated 180° out of phase with the first. The second layer can belong to another actuator or the opposite half of a bimorph actuator.

C. Drive Methods

Applying a drive signal to a unimorph or other dual-electrode piezoelectric actuator involves a single sinusoidal, unipolar source connected directly to the electrodes of the actuator, as shown in Fig. 2(a). Two methods of applying a drive signal to a bimorph are shown in Fig. 2(b) and (c). The method of Fig. 2(b), termed alternating drive, includes two sinusoidal, unipolar sources connected to the outer electrodes and operated 180° out of phase, with a common ground on the central electrode. The method of Fig. 2(c), termed simultaneous drive, consists of a constant high-voltage bias applied across the actuator and a sinusoidal, unipolar source connected to the central electrode. Alternating drive requires $2n$ sinusoidal sources per n bimorphs, while simultaneous

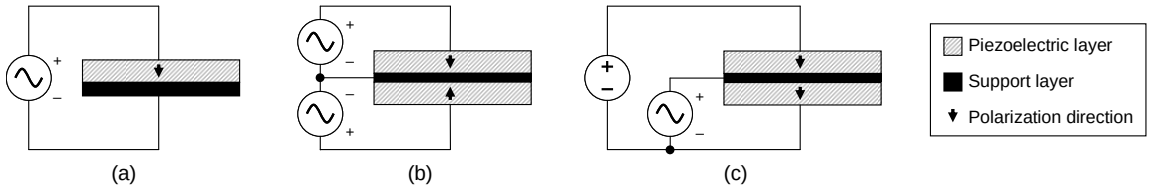

Fig. 2. Unipolar drive methods for piezoelectric actuators: unimorph (a), bimorph with alternating drive (b), and bimorph with simultaneous drive (c).

drive offers the possibility of sharing the high-voltage bias among multiple actuators and therefore requires n sinusoidal sources and one constant source per bimorph.

From a circuit design perspective, the sinusoidal sources can be implemented in two fundamental ways: a two-stage design, where the first stage steps up the low battery voltage to a high voltage and the second stage generates a time-varying drive signal; or a single-stage design, which simultaneously steps up the voltage and generates a time-varying signal. Since a two-stage design already generates a constant high-voltage output, it can easily be applied to the simultaneous drive method of Fig. 2(c), while a one-stage design is suitable for the alternating drive method of Fig. 2(b) and for dual-electrode actuators as in Fig. 2(a). Note that a two-stage design will generally have more components and larger weight, but will allow the sharing of the high-voltage bias. In contrast, a single-stage design will be more lightweight but cannot be shared. As a result, the selection of the drive method will depend on the number and type of actuators in a given system.

D. Prior Work

Several researchers have discussed the miniaturization of voltage conversion circuits for microrobotic applications. A brief introduction to promising topologies is given in [1] and [13], which note that commercially available voltage converters with the required capabilities weigh several grams, far above the weight budget of many microrobotic platforms. One of the circuits described in this paper is mentioned in [13]. So far, the smallest standalone voltage converter used in a microrobotic platform is a circuit described in [1], consisting of a standard boost converter and a voltage multiplier, and weighing about 200mg. However, the large number of discrete components reduces the power density of the design to around 250W/kg, which may be insufficient for the stringent power demands of flying microrobots [13].

Efficient high-voltage drive stages for piezoelectric actuators have likewise been the subject of several publications in the past decade [14], [15], [16], [17]. An overview of drive circuits can be found in [18]. The majority of these implementations are intended for large-scale, high-power applications, such as automotive actuators.

This work focuses on the miniaturization of high-voltage piezoelectric drive circuits to below 100mg. At such small scales, the effect of loss mechanisms becomes more pronounced, necessitating a careful selection of circuit topologies and control methods to maintain the high power density required by microrobotic applications while maximizing efficiency.

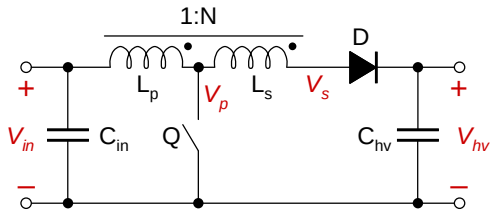

Fig. 3. Autotransformer boost converter.

III. Dual-Stage Drive Circuit

Switching power supplies, which combine passive components with active semiconductor switches in order to efficiently transfer small packets of energy from power source to load, are best suited for the level of miniaturization necessitated by microrobotic applications. A number of switching topologies have the ability to boost the input voltage to higher levels. However, as the voltage step-up ratio increases and the output power decreases, some topologies begin to suffer from growing component sizes and efficiency degradation. This section describes a dual-stage drive circuit consisting of a voltage conversion stage and drive stage, which may be used to drive one or more bimorphs as shown in Fig. 2(c).

A. Voltage Conversion Stage

The autotransformer boost converter, shown in Fig. 3, can be regarded as a combination of the well-known boost and flyback topologies [19]. As mentioned in [13] and [19], this topology offers a number of advantages over other boosting topologies for low-power, high voltage step-up ratio applications. The design also lends itself well to miniaturization, which can reduce the efficiency and/or manufacturability of other topologies [1].

When the switch transistor Q is turned on, current builds up in the primary winding L_p of the autotransformer. When Q is turned off, the energy stored in the magnetic core is discharged to the high-voltage output through both the primary and the secondary windings. Voltage and current waveforms of the converter are shown in Fig. 4. Further details of this topology can be found in [20].

The converter operates in discontinuous mode, where the autotransformer current must return to zero before a new switching cycle may begin. This mode of operation generally results in higher efficiency at low output power levels [21],

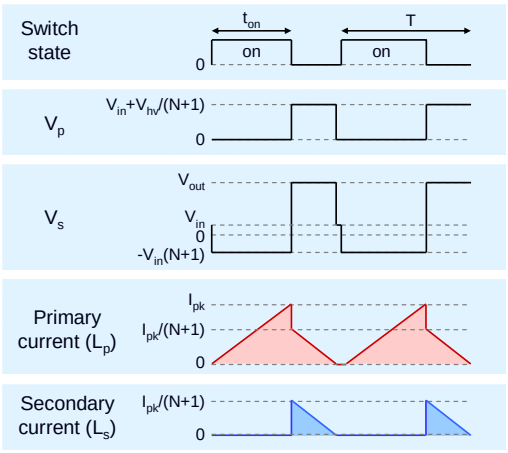

Fig. 4. Voltage and current waveforms during typical switching cycles for the autotransformer converter.

and simplifies the design of the control loop. In discontinuous mode, the voltage step-up ratio is given by:

$$\frac{V_{hv}}{V_{in}} = \frac{V_{in} t_{on}^2}{2TI_{out}L_p} + 1 \tag{1}$$

where V_{in} and V_{hv} are the input and output voltages, respectively, T is the switching period, I_{out} is the load current, t_{on} is the switch on-time, and L_p is the inductance of the primary winding of the transformer.

The output voltage is monitored using a resistive feedback divider and an analog comparator. When the output voltage falls beneath a certain threshold, the switch transistor is turned on until the inductor current reaches the predetermined level I_{pk}, delivering a quantity of energy (given by $L_p I_{pk}^2/2$) to the output. This control method naturally adjusts the frequency of charging pulses to regulate the output voltage at the desired level over a range of load currents.

B. High-Voltage Drive Stage

The high-voltage drive stage must be capable of producing a unipolar sinusoidal output and recovering charge from the load. A semiconductor half-bridge switching stage, while compact, can only produce a square-wave output and does not provide charge recovery [1]. Although a charge recovery method using an inductor and additional switches has been proposed [8], it can only transfer the charge all at once, which places a lower bound on the minimum size of the inductor and limits the circuit to quasi-square-wave driving. Another alternative involves using the half-bridge to generate a PWM output that can be filtered by an RC network consisting of a resistor and the intrinsic actuator capacitance to generate an arbitrary output waveform. In this case, however, a large amount of energy is dissipated in the resistor, limiting efficiency to under 50% before any other losses are considered.

The drive circuit in Fig. 5, found in many switching amplifiers, is a bidirectional buck-boost converter which operates in buck mode when delivering energy to the load and in boost mode when removing energy from the load. By using a theoretically lossless LC network consisting of an

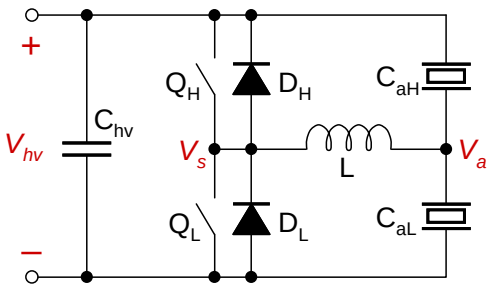

Fig. 5. Switching amplifier drive stage.

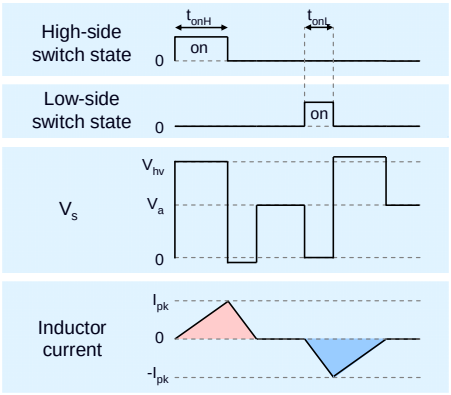

Fig. 6. Voltage and current waveforms during typical switching cycles for the switching amplifier.

inductor and the intrinsic actuator capacitance, this design is able to both generate an arbitrary unipolar output waveform and recover unused energy from the load. When the high-side switch Q_H is turned on, the inductor current begins to rise. When Q_H is turned off, the freewheel current through the diode D_L completes the delivery of charge to node V_a. Conversely, turning on the low-side switch Q_L removes charge from V_a and delivers it back to the supply, represented by capacitor C_{hv}, via the diode D_H. By issuing a sequence of charge and discharge pulses at appropriate times, an arbitrary waveform (in this case, a sinusoid) can be generated at V_a. The voltage and current waveforms for individual switching cycles are shown in Fig. 6. Unlike [8], only a small amount of energy is transferred during each switching cycle, which relaxes the constraints on the minimum inductor size.

The circuit is well-suited to driving bimorph actuators in the configuration of Fig. 5, where the two piezoelectric layers are represented by C_{aH} and C_{aL}. If C_{aH} is not present, the energy returned to supply C_{hv} when C_{aL} is discharged causes V_{hv} to rise. This complicates the regulation of V_{hv} and requires a large C_{hv} to reduce voltage transients. When C_{aH} is present, however, energy is simply transferred back and forth between C_{aL} and C_{aH}, and the voltage conversion stage that regulates V_{hv} needs only to compensate for losses in the actuator and drive stage. The size of C_{hv} can therefore be kept to a minimum.

C. Drive Stage Control Method

In low-power microrobotic applications, it is important to control the switching amplifier drive stage of Fig. 5 in a way that maximizes efficiency while generating the sinusoidal signal. The conventional approach to switching amplifiers uses the switch transistors to generate a PWM waveform, which is converted by the LC network into an output voltage equal to the average value of the PWM signal [22]. When connected to a primarily capacitive load with low energy dissipation, such an amplifier must actively charge and discharge the load during each switching cycle in order to maintain some voltage across the load [23]. This results in significant switching and conduction losses in the amplifier even when the output voltage is constant or changing slowly.

A method proposed in [23] involves transferring only the necessary amount of energy to or from the actuator during each switching cycle by turning on the high-side switch Q_H for an appropriate amount of time when the actuator needs to be charged, and the low-side switch Q_L when the actuator needs to be discharged. The outputs of two A/D converters, which sample the desired and actual values of the output voltage, are used to address a table of precomputed on-times for the switches, and the appropriate switch is then turned on for the prescribed length of time. A new charging cycle begins when the inductor current has returned to zero, which can be detected by monitoring the magnetization of the inductor as in [23], or the inductor current. This results in a simple, efficient, and cost-effective system with low computational requirements.

Here, the concept is simplified further. Because switching losses are frequently the dominant loss mechanism in high-voltage, low-power switching amplifiers, the inductor current is always allowed to reach a value of I_{pk} which is close to the saturation current limit of the inductor. This transfers the largest possible amount of energy during each switching cycle and reduces the total number of switching cycles necessary to fully charge or discharge the actuator. It also requires only 2^{N+1} precomputed on-times for an N-bit A/D resolution, vs. 2^{2N} as in [23]. However, the inability to select a lower I_{pk} to make fine adjustments in the output voltage reduces the smoothness of the output waveform.

Using the expressions for the energy stored in a capacitor ($CV^2/2$) and inductor ($LI^2/2$), it is straightforward to derive the expressions for the change in output voltage after a charging pulse and a discharging pulse. These are given by:

$$\Delta V_{chg} = \sqrt{V_a^2 + \frac{LI_{pk}^2}{C_a}} - V_a \tag{2}$$

$$\Delta V_{dchg} = \sqrt{V_a^2 - \frac{LI_{pk}^2}{C_a}} - V_a \tag{3}$$

where V_a is the amplifier output voltage, C_a is the actuator capacitance, L is the value of the inductor, and I_{pk} is the peak inductor current. Furthermore, the relationship between the constant voltage across an inductor and the time-varying current ($V = L\frac{di}{dt}$) can be used to compute the on-times for the high-side and low-side switches, t_{onH} and t_{onL}, that will result in a current I_{pk} in the inductor:

$$t_{onH} = \frac{LI_{pk}}{V_{hv} - V_a} \tag{4}$$

$$t_{onL} = \frac{LI_{pk}}{V_a} \tag{5}$$

where V_{hv} is the drive stage supply voltage and all other quantities are as defined above.

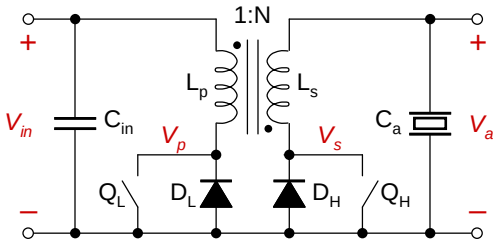

Fig. 7. Bidirectional flyback converter.

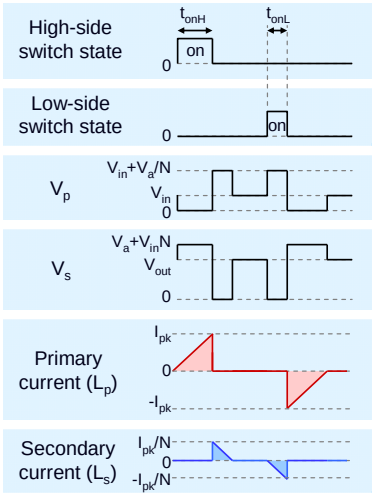

Fig. 8. Voltage and current waveforms during typical switching cycles for the bidirectional flyback converter.

The implementation of [23] includes a large capacitor in parallel with the piezoelectric actuator to reduce the effects of the nonlinear actuator capacitance and minimize voltage spikes in case of external mechanical stimulation of the actuator. Although the actuator capacitance is nonlinear, the dominant component of this capacitance, C_0, depends on the piezoelectric material thickness, which changes by less than 0.1% during normal actuation. Moreover, since microrobotic actuators will generally be driven near or below the lowest-frequency resonant mode of the mechanical system, the actuator capacitance will not change significantly and can be driven directly by the switching amplifier. However, high-voltage component ratings should include a safety margin to account for any external stimulation of the actuator.

IV. Single-Stage Drive Circuit

Most boosting power supply topologies can be adapted to produce a variable output voltage instead of regulating a

fixed output voltage, and many topologies are also capable of bidirectional power transfer in order to permit the recovery of energy from the load. Such topologies could be used in a single-stage circuit to drive a unimorph actuator, as in Fig. 2(a), or two such circuits could be used to drive a bimorph, as in Fig. 2(b).

The bidirectional flyback converter in Fig. 7 is a promising topology which shares many advantages with the autotransformer boost converter described in the previous section. To charge up the actuator, Q_L is turned on, causing the current in the primary winding of the transformer to rise. When Q_L is turned off, the energy in the transformer core is discharged into the output via the diode D_H. Q_H and D_L are used in a similar fashion to discharge the actuator. Voltage and current waveforms are shown in Fig. 8. Further details of this topology may be found in [24].

The control method of the bidirectional flyback converter is very similar to the drive stage described in the previous section. However, since the bidirectional flyback converter incorporates voltage step-up functionality, switching losses are no longer the dominant loss mechanism. As a result, the optimal value of I_{pk} may no longer be near the inductor saturation current limit; rather, a separate optimization is required to determine it. The expressions for the changes in output voltage during charging and discharging are determined as before:

$$\Delta V_{chg} = \sqrt{V_a^2 + \frac{L_p I_{pkC}^2}{C_a}} - V_a \tag{6}$$

$$\Delta V_{dchg} = \sqrt{V_a^2 - \frac{L_s I_{pkD}^2}{C_a}} - V_a \tag{7}$$

where V_a is the amplifier output voltage, C_a is the actuator capacitance, L_p and L_s are the inductances of the primary and secondary transformer windings, respectively, and I_{pkC} and I_{pkD} are the peak currents in the primary winding during charging and secondary winding during discharging, respectively. The on-times for the high-side and low-side switches, t_{onH} and t_{onL}, are given by:

$$t_{onH} = \frac{L_p I_{pkC}}{V_{in}} \tag{8}$$

$$t_{onL} = \frac{L_s I_{pkD}}{V_a} \tag{9}$$

where V_{in} is the input supply voltage and all other quantities are as defined above. By timing the charge and discharge pulses appropriately, this circuit can generate a sinusoidal waveform and recover unused energy from the actuator, similar to the switching amplifier drive stage described earlier.

V. Experimental Realization

To perform a high-level optimization of the drive circuits, a series of MATLAB scripts is developed to model various loss mechanisms as a function of circuit design parameters in the expected region of operation. The losses can be broadly categorized as conduction losses, which include the switch on-state resistances, the diode forward voltage drop, and the series resistance of magnetic components; switching losses, which include the energy required to charge the gate and output capacitances of the switches, switch turn-on and turn-off losses, and diode recovery losses; and finally, magnetic losses, which include hysteresis losses, eddy current losses, and the leakage inductance of transformers. The modeling of these loss mechanisms is described in more detail in [25]. The design parameters include transformer winding ratios N (Figures 3, 7), inductances L and L_p, peak current levels I_{pk}, and on-times t_{on}, t_{onH}, and t_{onL} (Figures 3, 5, 7). All electronic components are modeled on existing commercial devices, using manufacturer data to establish the expected ranges for device parameters.

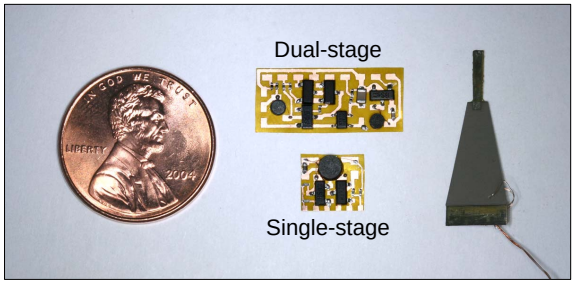

Fig. 9. Dual-stage driver and single-stage driver implemented on flex circuit next to a piezoelectric bimorph actuator.

The circuits described in Sections III and IV are implemented using discrete components on a custom flex circuit (Fig. 9). The block diagram of the dual-stage design, including the voltage conversion stage and the drive stage, is shown in Fig. 10. Although final implementations will include a custom, low-power integrated control circuit, an Atmega128 microcontroller with onboard ADC and analog comparator is used to implement the control functionality in the proof-of-concept implementations. Since the weight and power consumption of the Atmega128 do not form an accurate representation of an efficient control circuit, they are excluded from weight and efficiency calculations.

Custom miniature transformers are fabricated using ferrite bobbin cores salvaged from the Coilcraft LPS3015 and LPS4018 series of surface-mount inductors. The unshielded cores weigh 10mg and 30mg, respectively, which allows extremely lightweight magnetics. Several winding strategies have been investigated, with the highest coupling coefficients resulting from arranging the windings in three layers that run along the entire length of the bobbin, with the primary winding occupying the middle layer and the secondary winding occupying the inner and outer layers. The transformers used in the single-stage driver and the DC conversion stage of the dual-stage driver have primary inductances of 10-12μH, turns ratios of 11 to 13, series resistances of 20-40Ω, and coupling coefficients of 0.9 to 0.95. The flex circuit was fabricated using a copper-laminated polymer film. The pins of integrated circuit packages were shortened to minimize weight.

Two versions of the autotransformer voltage converter,

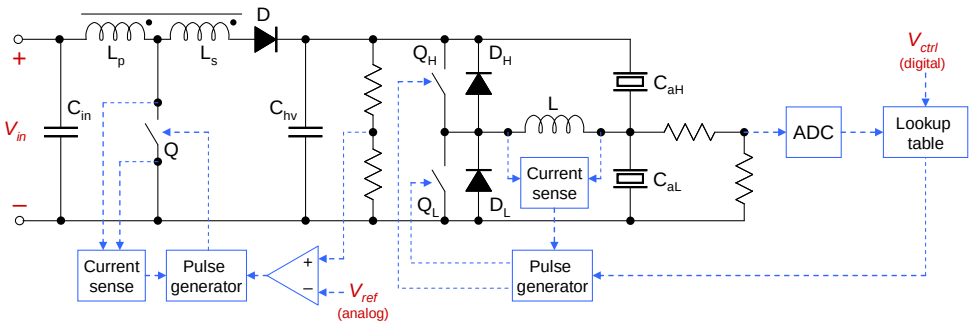

Fig. 10. Dual-stage power electronics block diagram, consisting of the voltage conversion stage, the drive stage, and control loops.

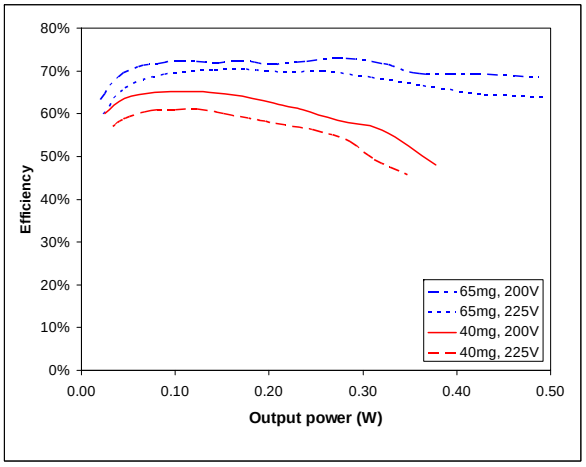

Fig. 11. Efficiency of voltage conversion stages using different transformer cores at 3.7V input, 200V and 225V output.

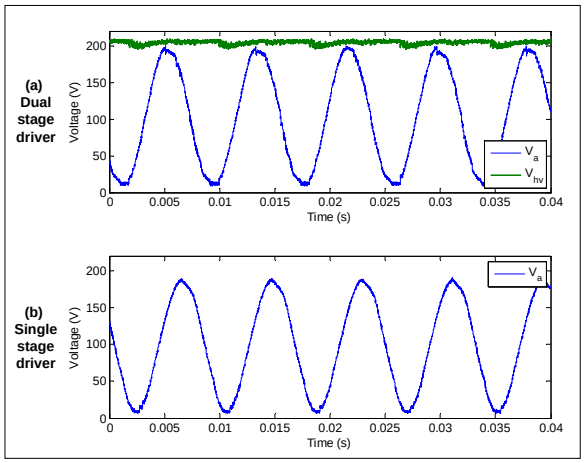

Fig. 12. Oscilloscope traces for the dual-stage driver (a) and single-stage driver (b).

weighing 40mg and 60mg, are implemented using different transformer cores. The lighter and heavier versions are capable of power outputs of up to 380mW and 500mW, respectively, resulting in power densities of 9500W/kg and 8300W/kg before considering control circuits. The measured efficiency of the converters at a 3.7V input voltage, typical of lithium polymer batteries, and output voltages of 200V and 225V, is shown in Fig. 11. The converters were optimized for 100-150mW output power, and as a result the peak efficiency occurs in this operating region.

The complete dual-stage drive circuit weighs 90mg as constructed, which includes the 40mg voltage conversion stage and a 50mg drive stage. Scope traces produced by the dual-stage circuit are shown in Fig. 12(a). Here, the circuit is driving two 22nF capacitors, representing a piezoelectric bimorph, with a 205V high-voltage bias and a 200V sinusoidal signal at 120Hz. These drive conditions result in a current draw of 46mA from a 3.7V supply. By contrast, an identical drive stage with the inductor replaced by a resistor draws 83mA, while the weight of the circuit is reduced by only 10mg. By increasing the output power to the maximum possible value at higher output frequencies, the aggregate power density of the dual-stage circuit is found to be over 1800W/kg.

The operating frequency in Fig. 12(a) is higher than typical flapping frequencies for wings powered by bimorphs of the size shown in Fig. 9, which are on the order of 40-80Hz, and a 22nF capacitance is about 1.5 times greater than the primary capacitance C_0 of such bimorphs. This indicates a significant safety margin in the output power of the circuit. Fig. 13 shows high-speed video frames of the wing flapping motion powered by the dual-stage drive circuit. The flapping angle is about 110°, similar to previous results [4].

Using a similar controller setup, experimental results for a 60mg single-stage circuit are also presented. The scope trace produced when driving a 22nF capacitor with a 190V, 120Hz sinusoidal signal is shown in Fig. 12(b). The output signal amplitude is slightly lower than the dual-stage circuit output due to the maximum voltage ratings of the switch transistors. For these drive conditions, the current draw from a 3.7V supply is 10mA. The power density of the single-stage circuit is over 1600W/kg. The power circuits described in this paper represent, to the authors' best knowledge, the highest efficiency and power density attained in a sub-100mg high-voltage power electronics package so far.

VI. Summary and Future Work

This paper describes the design and implementation of milligram-scale high-voltage power electronics circuits suit-

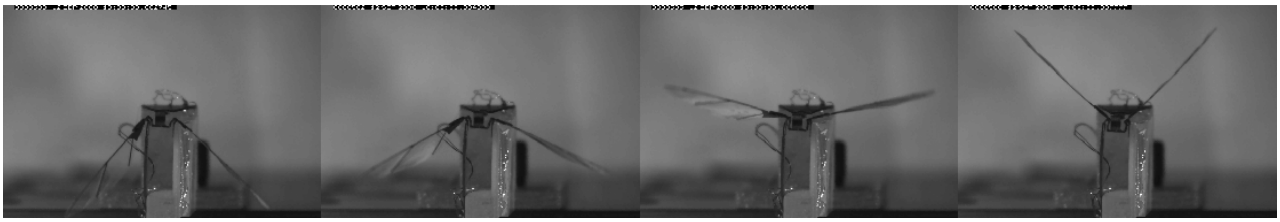

Fig. 13. High-speed video frames of the flapping motion of fly wings when the actuator is driven with the dual-stage circuit.

able for driving piezoelectric actuators in a variety of compact applications, including autonomous microrobots. The electrical behavior of piezoelectric actuators is discussed and used to establish optimal drive requirements. Circuit topologies suitable for driving piezoelectric bimorphs, as well as dual-electrode actuators such as unimorphs and stacks, are presented. The experimental realizations of the circuits are described, which include sub-100mg voltage converters and high-voltage drivers with step-up ratios of up to 60, power densities of over 1600W/kg, and the ability to generate an arbitrary output signal and recover energy from the load. The applicability of the drive circuits to a flapping wing robotic insect, such as the Harvard Microrobotic Fly, is verified by demonstrating successful wing flapping motion powered by one of the drive circuits.

Future work will focus on the continued optimization and miniaturization of the power electronics circuits, including ways to boost efficiency through such circuit techniques as soft switching [26]. On the implementation side, efforts will be directed towards the fabrication of custom ferrite magnetic components to replace the current devices constructed from disassembled commercial parts, in order to improve coupling, reduce weight, and minimize electromagnetic interference. In order to reduce the weight of the power electronics package even further, bare-die versions of the power semiconductors will be used, which may require the deencapsulation of existing components from the package if bare-die versions cannot be obtained from manufacturers. Finally, the design and fabrication of a custom, low-power integrated circuit which implements the required control functionality is a necessary milestone in developing a standalone system suitable for integration in an autonomous microrobotic platform.

REFERENCES

[1] E. Steltz, M. Seeman, S. Avadhanula, and R. S. Fearing, "Power electronics design choice for piezoelectric microrobots," in *IEEE/RSJ Int. Conf. on Intelligent Robots and Systems*, 2006, pp. 1322–1328.

[2] S. Hollar, A. Flynn, C. Bellew, and K. S. J. Pister, "Solar powered 10 mg silicon robot," in *Proc. IEEE Sixteenth Annual Int. Conf. on Micro Electro Mechanical Systems*, 2003, pp. 706–711.

[3] R. D. Kornbluh, R. Pelrine, Q. Pei, R. Heydt, S. Stanford, S. Oh, and J. Eckerle, "Electroelastomers: Applications of dielectric elastomer transducers for actuation, generation, and smart structures," in *Proc. SPIE*, vol. 4698, 2002, pp. 254–270.

[4] R. J. Wood, "Liftoff of a 60mg flapping-wing MAV," in *IEEE/RSJ Int. Conf. on Intelligent Robots and Systems*, 2007, pp. 1889–1894.

[5] A. Schneuwly, "Charge ahead (ultracapacitor technology and applications)," *Power Engineer*, vol. 19, pp. 34–37, February 2005.

[6] C. L. Bellew, S. Hollar, and K. S. J. Pister, "An SOI process for fabrication of solar cells, transistors and electrostatic actuators," in *IEEE Int. Solid-State Sensors and Actuators Conf.*, June 2003, pp. 1075–1078.

[7] A. Wilhelm, B. W. Surgenor, and J. G. Pharoah, "Evaluation of a micro fuel cell as applied to a mobile robot," in *IEEE Int. Conf. on Mechatronics and Automation*, 2005, pp. 32–36.

[8] D. Campolo, M. Sitti, and R. S. Fearing, "Efficient charge recovery method for driving piezoelectric actuators with quasi-square waves," *Ultrasonics*, vol. 50, no. 3, pp. 237–244, March 2003.

[9] R. J. Wood, E. Steltz, and R. S. Fearing, "Optimal energy density piezoelectric bending actuators," *Sensors & Actuators: A. Physical*, vol. 119, no. 2, pp. 476–488, 2005.

[10] M. Guan and W.-H. Lao, "Studies on the circuit models of piezoelectric ceramics," in *Int. Conf. on Information Acquisition*, 2004, pp. 26–31.

[11] S. Sherrit, H. D. Wiederick, and B. K. Mukherjee, "Accurate equivalent circuits for unloaded piezoelectric resonators," in *IEEE Ultrasonics Symposium*, 1997, pp. 931–935.

[12] R. Sahai, S. Avadhanula, R. Groff, E. Steltz, R. Wood, and R. Fearing, "Towards a 3g crawling robot through the integration of microrobot technologies," in *IEEE Int. Conf. on Robotics and Automation*, 2006.

[13] M. Karpelson, G.-Y. Wei, and R. J. Wood, "A review of actuation and power electronics options for flapping-wing robotic insects," in *IEEE Int. Conf. on Industrial Tecnhnology*, 2008, pp. 779–786.

[14] W. M. Zavis and W. E. Shanks, "Design advances for high-efficiency regenerative piezoelectric drive amplifier," in *Proc. SPIE*, vol. 4327, 2001, pp. 118–124.

[15] D. J. Clingman and M. Gamble, "High voltage switching piezo drive amplifier," in *Proc. SPIE*, vol. 3674, 1999, pp. 280–286.

[16] J. Luan, "Design and development of high-frequency switching amplifiers used for smart material amplifiers used for smart material actuators with current-mode control," Ph.D. dissertation, Virginia State University, 1998.

[17] G. Gnad and R. Kasper, "Power drive circuits for piezo-electric actuators in automotive applications," in *IEEE Int. Conf. on Industrial Tecnhnology*, 2006, pp. 1597–1600.

[18] G. Gnad, "Ansteuerkonzept fur piezoelektrische Aktoren," Ph.D. dissertation, University of Magdeburg, 2005.

[19] "Small, high-voltage boost converters," Maxim Semiconductor Application Note 1109, 2002.

[20] N. Vazquez, L. Estrada, C. Hernandez, and E. Rodriguez, "The tapped-inductor boost converter," in *IEEE Int. Symposium on Industrial Electronics*, 2007.

[21] X. Liu, S. Guo, S. Wang, F. Xu, G. Du, and Y. Chang, "Analysis and design of a high efficiency boost DC-DC converter based on pulse-frequency modulation," in *Int. Symposium on Integrated Circuits*, 2007, pp. 398–401.

[22] "Class D audio amplifier basics," International Rectifier Application Note AN-1071.

[23] H. Janocha and C. Stiebel, "New approach to a switching amplifier for piezoelectric actuators," in *Actuator 98*, pp. 189–192.

[24] K. Venkatesan, "Current mode controlled bidirectional flyback converter," in *IEEE Power Electronics Specialists Conf.*, 1989, pp. 835–842.

[25] A. Pressman, *Switching Power Supply Design*. McGraw-Hill Professional, 1998.

[26] G. Spiazzi, D. Tagliavia, and S. Spampinato, "DC-DC flyback converters in the critical conduction mode: a re-examination," in *IEEE Industry Applications Conf.*, vol. 4, 2000.